European Journal of
Nuclear
Medicine

Review article

Collimator design for single photon emission tomography

Stephen C. Moore[1], Kypros Kouris[2] and Ian Cullum[2]

[1] Department of Biomedical Engineering, Worcester Polytechnic Institute, 100 Institute Road, Worcester, MA 01609, USA
[2] Institute of Nuclear Medicine, University College and Middlesex School of Medicine, Middlesex Hospital, Mortimer Street, London W1N 8AA, UK

Abstract. We discuss recent trends in collimator design and technology, with emphasis on theoretical and practical issues of importance for single photon emission tomography (SPET). The well-known imaging performance parameters of parallel-hole collimators are compared with those of fan-beam collimators, which have enjoyed considerable success in recent years, particularly for brain SPET. We review a simplistic approach to the collimator optimization problem, as well as more sophisticated "task-dependent" treatments and important considerations for SPET collimator design. Practical guidance is offered for understanding trade-offs that must be considered for clinical imaging. Finally, selective comparisons among different SPET systems and collimators are presented for illustrative purposes.

Key words: Collimators – SPET – Multi-headed cameras

Eur J Nucl Med (1992) 19:138–150

The need for a collimator

With visible light, an image is formed using mirrors and/or lenses to bend and focus the light photons, thereby guiding them along a precise path to a recording device. Gamma-rays cannot be focussed in the optical sense, but for an image to be formed a similar principle must be obeyed, namely that there must be a one-to-one correspondence between the direction of emission of a gamma-ray from a radioactive source and its point of detection. The collimator or coded aperture in single-photon imaging and the electronic collimation of the annihilation gamma-rays in positron imaging are the means for achieving this requirement. Unfortunately, most of the gamma-rays emitted during the data acquisition time do not travel in the direction(s) allowed by the collimator(s) and therefore do not contribute to image formation. For this reason, radionuclide imaging is a photon limited process, e.g. for single photon imaging, typically only 1 in about 10^5 emitted gamma-rays is detected.

In planar imaging using a gamma-camera, the three-dimensional (3-D) distribution of activity in the organ or tissue of interest is represented as a two-dimensional (2-D) image, called a view or projection in a specified direction. For the case of a parallel-hole collimator (Fig. 1), each point on such a projection image has, in principle, a value equal to the number of detected gamma-rays that travelled through the corresponding collimator hole. In the absence of scattering, the detection of a gamma-ray would convey the information that a radioactively labelled molecule had existed somewhere along the line through the collimator hole and that it had disintegrated during the imaging time interval. The position, i.e. the depth, of the labelled molecular along the line is not known.

The objective in single photon emission tomography (SPET) is to derive the 3-D distribution of the radiopharmaceutical in the organ or tissue of interest (Heller and Goodwin 1987). Using collimators, the 3-D problem is reduced to that of reconstructing one or a series of images of different slices. The slice(s) are physically defined by the collimators so that the acquired data are identified as arising from particular slice(s). The most common device for SPET is the rotating Anger gamma-camera fitted with a parallel-hole collimator. With the gamma-camera parallel to the axis of rotation, a series of projections are acquired at equally spaced angles. Neglecting the geometric divergence with depth due to the finite size of the collimator holes, the pixel data of a particular row in each projection may be assumed to arise from a single slice, the slice being parallel to the row and perpendicular to the face of the gamma-camera. Information on the depth of sources within a given slice is obtained by reconstructing all the angular projection data for that slice.

SPET using a single rotating gamma-camera has gained a wide role in clinical practice and research, particularly in heart studies (Hor 1988). Systems with more than one camera on a rotating gantry (multi-headed systems) or with an array of detectors (multi-detector systems) have been introduced in order to increase the number of lines along which gamma-rays can be de-

Offprint requests to: S.C. Moore

tected simultaneously (Lim et al. 1986; Budinger 1990). Thus, the efficiency of the imaging process, i.e. the sensitivity, is significantly increased. This improved efficiency can then be traded off for improved spatial resolution (with lower efficiency) by using high-resolution collimators.

Collimator design parameters and manufacturing considerations

Figure 1 depicts in one dimension the relevant geometry for imaging a point source with a NaI(Tl) crystal detector, as seen through the collimator. Of course, in reality collimation is performed in both dimensions within the imaging plane (as discussed above), and the "slits" between the septa in Fig. 1 represent, in fact, long holes through a slab of material covering the entire camera crystal. Viewed from the point source, the entrance plane of the collimator usually appears as a close-packed array of hexagonally shaped holes, although other hole shapes and packing patterns are also used. The most important design parameters are: *a*, the thickness of the collimator (i.e. the length of the holes through the collimator); *d*, the diameter of the holes (or, for hexagonal holes, the perpendicular "face-to-face" distance); *s*, the thickness of the septal material; and, finally, the material used to make the collimator. The effects of the collimator design on important image quality indicators, such as resolution and sensitivity, will be discussed in the next section.

It is desirable to use a septal material with a high linear attenuation coefficient through the relevant energy range. (With a higher linear attenuation coefficient, the septa can be made thinner, thus allowing improved geometric efficiency for a fixed resolution and fixed fraction of photons penetrating the septa.) Most collimators are made of lead, although recently some have been fabricated from tungsten and tantalum, but at much greater cost. Lead collimators have historically been manufactured by stamping thin sheets of lead foil into half-hexagonal, corrugated sheets and then stacking up the corrugated sheets, with careful attention to hole alignment. More recently, improved techniques have been developed for casting collimators by pouring molten lead into molds. High-resolution foil collimators have been manufactured with somewhat thinner septal walls ($\sim$0.15 mm) than currently seem to be manufacturable with cast collimators ($\sim$0.3 mm); however, the uniformity of the cast collimators is generally better than that of the foil collimators, which can suffer from regional variations in efficiency and "channel tilt" (Chang et al. 1988). For this reason, Gillen et al. (1988) recommended the use of cast collimators, especially for SPET applications. With either foil or cast collimators, however, careful handling is essential. In practice, the uniformity of a collimator is most likely to be affected adversely by inadvertently denting the surface with small, hard

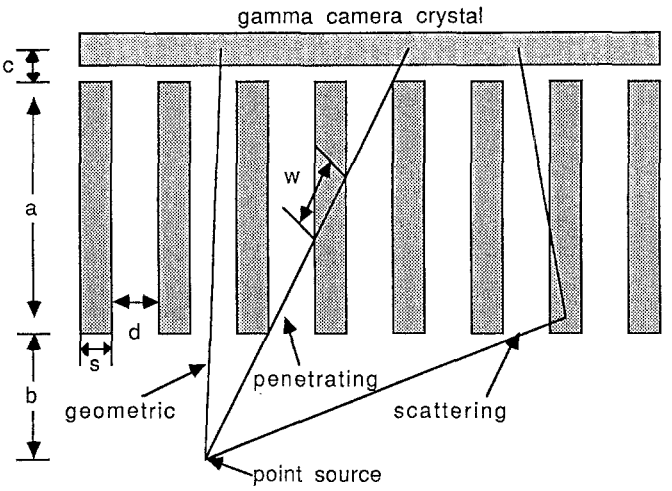

Fig. 1. Schematic and notation used for a parallel-hole collimator

objects. It has been demonstrated (Jarritt and Ell 1984) that uncorrected uniformity "blemishes" on the camera or collimator surface can cause significant "ring" artifacts in reconstructed SPET images.

Another important practical consideration for SPET is the weight of the collimator. Some SPET systems employ a counterbalancing technique for offsetting the weight of the collimator and camera to minimize risks to the patient and to reduce the load on the gantry's rotational motor. The method used for counterbalancing on any given SPET system may restrict the range of acceptable collimator weights. This must be kept in mind when considering the use of alternative collimators.

Review of collimator performance parameters

The collimator limits the performance of a nuclear medicine imaging system more than any other single component. As such, it is important to review briefly the relationship between parameters affecting image clarity and the collimator's geometric design. The spatial resolution, efficiency and penetration fraction of a parallel, multihole collimator were discussed first by Anger (1964). The geometric parameters of such a collimator are depicted in Fig. 1, along with three types of events which should be considered. The desirable, geometrically collimated gamma-rays traverse the collimator entirely within a hole, without contacting the septal material. Penetrating gamma-rays go through one or more septal walls without interacting, while scattered photons are deflected into the Anger camera by a Compton or coherent interaction in a septum. The collimator penetration and scatter components are generally undesirable because their point of origin in the source is not necessarily directly under their point of detection in the Anger camera. Large numbers of penetrating or scattering photons can contribute a substantial background to the image, thereby degrading the contrast of important image features.

Spatial resolution

The spatial resolution of a parallel-hole collimator, expressed as the full width at half-maximum (FWHM) of the point spread function (PSF), is approximately:

$$r_c = d(a_e + b + c)/a_e \quad (1)$$

where d is the collimator hole size (Fig. 1), a is the collimator thickness, a_e is the effective collimator thickness ($a_e = a - 2/\mu$, where μ is the total linear attenuation coefficient of the collimator material at the relevant energy), b is the source-to-collimator distance, and c is the mean interaction depth in the detector. This formula was modified from that presented by Anger (1964) by considering that the collimator hole length, a, should be reduced on both ends by approximately $1/\mu$ due to penetration effects (Mather 1957; Gerber and Miller 1974); the value of $2/\mu$ for lead and technetium-99m is 0.9 mm.

Of course, the single parameter, r_c, in Eqn. (1) above does not offer a complete description of the collimator's PSF or its Fourier transform, the modulation transfer function (MTF), whose detailed shapes depend upon the shape of the collimator holes. Nevertheless, it has been argued (e.g. Muehllehner et al. 1976) that the exact shape of the collimator holes has only a small influence on the collimator's average transfer function, compared with the choice of the geometric parameters, especially d and a. These authors demonstrated small differences between the PSFs and MTFs of triangular and hexagonal hole shapes. Metz et al. (1980) derived exact expressions for the geometric component of the collimator MTF for *any* hole shape which confirmed these results and, additionally, treated circular and square holes. Both of these analyses used response functions averaged over the appropriate periodic "cell size" of the collimator structure.

It is clear from Eqn. (1) above that the spatial resolution of the collimator worsens linearly with increasing distance from the collimator face. Also, it should be noted that the resolution changes *less* over a given range of collimator-source distances, b, for *larger* values of collimator thickness, a. In other words, the slope of the resolution vs. distance line is less for thicker collimators. Both of these observations have consequences for SPET imaging.

The overall resolution of a gamma-camera image is given by the 2-D convolution of the collimator PSF with the intrinsic gamma-camera's PSF. The intrinsic PSF is usually well approximated by a radially symmetric Gaussian function, with a FWHM, r_i, of $\sim$3–4 mm for a modern Anger camera. For the sake of simplicity, if we also approximate the collimator's PSF by a Gaussian function, then the combined *system* spatial resolution is approximately given by the quadrature sum:

$$r_s \approx (r_c^2 + r_i^2)^{1/2} \quad (2)$$

It may be seen that for virtually all collimators used to date in nuclear medicine studies, the overall system resolution is dominated by the collimator resolution.

Geometric efficiency

The collimator's geometric efficiency is simply the fraction of isotropically emitted gamma-photons which are appropriately collimated. This efficiency is effectively independent of the source to collimator distance (under usual imaging conditions) and is given by:

$$g = k\{d^2/[a_e(d+s)]\}^2 \quad (3)$$

where k is a factor which depends upon the hole shape and pattern (k = 0.263 for hexagonal, closely packed holes), and a_e, d and s are defined in Fig. 1 and Eqn. (1). The collimator's efficiency determines the number of gamma-ray counts that may be recorded for a given source distribution of radioactivity in a given scan time (often called "count sensitivity"). Since the relative statistical noise of the image decreases as the square root of the number of image counts, collimator efficiency is an important consideration. Note that either shortening the collimator hole length, a, or decreasing the septal thickness, s, increases the collimator efficiency, while decreasing the hole size, d, decreases the efficiency. It can be shown from Eqns. 1 and 3 that in most practical situations the sensitivity will degrade approximately as the square of the geometric spatial resolution.

Resolution and sensitivity of fan-beam collimators

When imaging activity distributions smaller than the field of view (FOV) of the gamma-camera, significant performance gains may result from magnifying the object distribution to "fill" more of the camera's FOV. This can be accomplished using fan-beam collimators (e.g. Jaszczak et al. 1979), which are quite useful for SPET applications. Fan-beam collimators focus in one dimension to a "focal line" parallel to the axis of rotation of the gamma-camera on the other side of the patient, at focal length, f (Fig. 2). The reconstruction procedure for SPET is quite similar to that used for fan-beam CT scanners. Astigmatic collimators, which focus to two different focal lines in the two orthogonal directions, and cone-beam collimators, which focus to a point, may also be used for SPET (Jaszczak et al. 1986); however, projection data from these types of collimators are incompletely sampled, which can result in image distortions when reconstructing with linear reconstruction algorithms (Gullberg et al. 1991).

The performance parameters of a fan-beam collimator may be calculated from the work of Moyer (1974). Consider the point source shown in Fig. 2. For a fan-beam collimator, the photons emitted from the source will be collimated into one (or a few) hole(s) along the direction shown at angle θ. The FWHM of the *system*

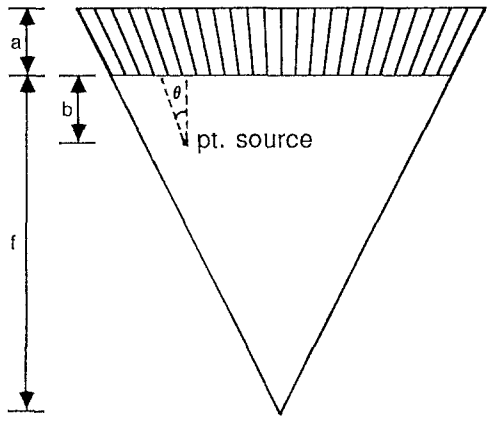

Fig. 2. Schematic and notation used for a fan-beam collimator

spatial resolution in the direction of the fan is given by the quadrature sum:

$$r_s = \{r_o^2 + [r_i(f-b)/(f+a_e+c)]^2\}^{1/2} \quad (4)$$

where the intrinsic camera resolution has been reduced (improved) by the "minification factor", $(f-b)/(f+a_e+c)$, between the detector image and the object plane at depth, b. The effects of the collimator resolution (also after minification to the object plane) are included in r_o which was shown by Moyer (1974) to be the product of three factors:

$$r_o = [d(a_e+b+c)/a_e] \times (1/\cos\theta) \times [1-(c+a_e/2)/(f+a_e+c)] \quad (5)$$

The first factor is simply the collimator resolution, r_c, for a parallel-hole collimator [Eqn. (1)]. The second factor results from the hole angulation, and the third arises from the minification to the object plane (the focussing effect).

The efficiency of a fan-beam collimator may, likewise, be related to that of a parallel-hole collimator. A modification of Moyer's formula (Ichihara 1990) gives:

$$g_{fan} = g[\cos^2\theta][f/(f-b)] \quad (6)$$

where g is the efficiency of a parallel-hole collimator [Eqn. (3)]. The first modifying factor, $\cos^2\theta$, results from the increased length of the holes at larger angles. The last factor is the ratio of the linear extent of any source viewed by the collimator at a depth b to the extent of the same source against the collimator face.

From the equations above, it may be observed that both the system resolution and the imaging efficiency can be improved through the use of a fan-beam collimator. Although the resolution deteriorates with increasing source to collimator distance for both parallel and fan-beam collimators, it deteriorates less for the fan-beam (Tsui et al. 1986). For a point source in air, the sensitivity of a parallel-hole collimator is depth independent, but that of a fan-beam collimator increases as the source moves away from the collimator face, closer to the focal line.

Septal penetration

An analytical expression for the septal penetration contribution to the collimator PSF has not been developed; however, several investigators have successfully used numerical ray-tracing methods to examine the penetration component (Muehllehner and Luig 1973; Beck and Redtung 1985; Newiger and Jordan 1985). Most collimator designers have used an ad-hoc "rule" allowing a certain small fraction of gamma-rays to penetrate along the minimum path length through a single septum (e.g. Keller 1968). This minimum path length, w, is shown for the penetrating photon in Fig. 1 and is approximately given by:

$$w = sa/(2\,d+s) \quad (7)$$

for most practical collimators for which $a >> 2\,d+s$. If one specified an allowable penetration probability of, for example, 5% along this minimum path length ($e^{-\mu w} = 0.05$, or $\mu w = 3$), then this condition may be used to provide a constraint equation relating septal thickness, hole size and bore length:

$$s = 6\,d/(a\mu - 3) \quad (8)$$

Using typical values from Table 1 for a high resolution lead collimator, this equation yields a required minimum septal thickness for ^{99m}Tc of 0.12 mm. Other investigators (e.g. Kibby 1969) have suggested a stricter limitation on the probability of single septum penetration; nevertheless, the basic principle is the same. Of course, the allowable penetration fraction should ultimately be dictated by the imaging task we are trying to accomplish, as we shall discuss below.

If one insists upon an extremely low penetrating gamma fraction, then Eqn. (8) implies that the collimator septa will be rather thick for high energy isotopes. When the collimator hole spacing, $d+s$, becomes large compared with the intrinsic resolution of the gamma-camera, then the collimator structure (hole pattern) can become a visible and distracting artifact in the images (Newiger and Jordan 1985). This effect has also been considered using a generalized collimator transfer function (Beck and Redtung 1985). Collimator designers should be aware of this consideration, especially for high-energy isotopes. Most collimators used in recent years for SPET have been designed with resolution and penetration requirements which automatically render the collimator structure invisible in the image. However, further improvement in intrinsic gamma-camera resolution (to approximately 2.5 mm or better) would cause even these septa to be visualized. This subject will not be considered further in this article.

Collimator scatter

An analytic or numerically evaluable description of the collimator scatter component has eluded researchers.

Mather (1957) calculated the approximate scatter fraction for a single hole through a slab of material; however, this calculation is by no means straightforward when considering multi-hole collimators or multiple scattering. Another method of obtaining these response functions is by the use of Monte Carlo simulation (Raeside 1976), which is ideally suited to situations involving probability distributions (such as the angle of scatter for a Compton interaction). The basic method involves 'tracing' the photon path from its point of emission until detection or absorption occurs. The probabilistic nature of the transport is simulated by the use of random numbers. The method can accurately predict collimator response functions, taking account of scattering and any required geometry, and has been widely used in photon transport calculations. A disadvantage is that the calculation of collimator scatter PSFs can be extremely time-consuming because of the very low probability of photons surviving the collimator; however, deVries et al. (1990) recently described a Monte Carlo programme which accelerates such a simulation by propagating 1024 photons in parallel using an array processor, as well as by using several variance reduction techniques. These authors showed that the total collimator scatter contribution for a low-energy, general-purpose (LEGP) collimator is only $\sim$1.9% using a 20% energy window placed symmetrically about the ^{99m}Tc photopeak at 140 keV.

A practical measurement of the effect of the collimator on gamma-camera performance showed sensitivity changes on the order of 1%–2% in corresponding pixels with and without the collimator present (Cullum et al. 1991). The pattern of sensitivity variation, with greatest changes seen at photomultiplier tube centres, was similar to that when the camera was wrongly peaked for energy. This suggests the effect to be mainly due to scattering from the collimator.

Collimator scatter is a greater concern when imaging low- or medium-energy isotopes which also emit higher-energy "contaminant" photons, such as iodine-123 or indium-111. These higher-energy photons can scatter in the collimator, lose energy and be detected in the desired lower energy window of the gamma-camera. Simulating mono-energetic sources, deVries et al. (1990) reported collimator scatter fractions of 27% and 33% respectively, for 320 keV (chromium-51) and 514 keV (strontium-85) radiation incident on the LEGP collimator, detected in an ^{123}I energy window. For a medium-energy collimator, the corresponding collimator scatter fractions were 18% and 48%, respectively, for 320 keV and 514 keV incident radiation. Extrapolation of the ME data suggests that approximately 1.5% of the photons detected from a pure sample of ^{123}I (in air) in a window centred at 159 keV in fact arise from high-energy gamma-emissions in the range 346–538 keV. Contamination with ^{124}I at a level of 5% would cause the contribution from scattered photons to rise to approximately 6%. If the radioactivity were uniformly distributed in an absorbing material (e.g. a patient), the 159-keV gamma-emissions would be attenuated significantly more than the higher-energy contaminants, in which case the fraction of detected collimator scatter could be considerably larger than the scatter fractions estimated above from simulations of point sources in air.

Performance trade-offs in collimator design

It is evident from Eqns. (1), (3), and (7) that a variation in any one collimator geometric parameter affects resolution, efficiency and penetration in different ways. For example, given a fixed septal thickness and hole size, increasing the collimator thickness, a, will improve the spatial resolution and reduce septal penetration while decreasing the collimator's efficiency. Therefore, collimator design consists of determining the optimal trade-off among these various performance parameters for a given task to be accomplished by the imaging procedure.

Complex task specifications will be considered in the next section. A somewhat simplistic procedure, first described by Keller (1968), has been used by many collimator designers and will be briefly discussed here. Assuming that the desired spatial resolution is specified at an appropriate depth in the patient and that a given probability of single-septal penetration (e.g. 5%) is considered acceptable, then Eqns. (1) and (8) may be used with Eqn. (3) to eliminate any two of three parameters. For example, using Eqns. (1) and (8) to write d and s in terms of the other parameters, we can write the square root of the collimator efficiency as:

$$g^{1/2} = \mathrm{k}\,[r_c/(a_e+b+c)]\,[(a\mu-3)/(a\mu+3)] \qquad (9)$$

In this equation, the collimator thickness, a, is the only remaining free parameter. One can then maximize the collimator's geometric efficiency by setting to zero the derivative of Eqn. (9) with respect to a and then solving the resulting equation for a. For this case, the optimal collimator thickness is given by:

$$a_{\mathrm{opt.}} = \{[6\mu(b+c)+6]^{1/2}+3\}/\mu \qquad (10)$$

The optimal hole size, d, and septal thickness, s, may then simply be determined by using the optimal value of a in Eqns. (1) and (8), in turn.

It is important to understand the assumptions and limitations of the method just described. First, the procedure does not take into account the detailed *shape* of the point spread function or its components but rather treats only the FWHM of the geometric component and the fraction of allowed single-septum penetration. Second, collimator scatter is not included at all. (In practice, this may only be a significant concern when imaging certain isotopes, as discussed above.) Finally, it is assumed that the optimal spatial resolution and single-septal penetration fraction are already known for the appropriate imaging task.

Some criteria for optimization

Quantification of activity or size

One potential advantage of nuclear medicine, in comparison with other, more morphological imaging techniques, is the capability of deriving quantitative information such as the amount of a radiolabelled tracer taken up by a given organ or tumour. This is particularly true for SPET, as opposed to planar scintigraphy, because the activity in a structure of interest is easier to separate from that of the surrounding background when using a tomographic imaging technique. Even in SPET, however, the images are blurred by the system PSF, so that a finite spatial resolution will degrade the contrast of any lesions of a size less than ~3 times the system resolution. This consideration suggests the desirability of collimators with better spatial resolution. On the other hand, the degree of image noise will affect the precision with which activity may be estimated, which suggests the desirability of collimators with high efficiency. What is the optimal collimator design for quantification?

This question was recently addressed by Mueller et al. (1990), who used a maximum-likelihood (ML) technique to obtain quantitative information from planar images and compared this technique with the more traditional method of simply calculating the average and standard deviation of the total counts in a user-defined "region of interest" (ROI) on the images. The source model investigated was a small disc-shaped lesion, inside a larger, disc-shaped background. The image was blurred by a stationary Gaussian PSF, and random Gaussian noise was added. An ML fitting programme was then used to fit for the activities of the lesion and background, as well as the size (radius) of the lesion, over hundreds of images with differing noise levels. The ML estimate was accurate for all lesion sizes. For lesions of a size less than 1.5–2.0 times the FWHM of the PSF, the ROI estimate was highly inaccurate, yet more reproducible than that of the ML estimate, as expected. A figure of merit was defined as the standard error of each fitting parameter, expressed as a percentage of the true (known) parameter value. By varying the FWHM of the PSF and assuming that the pixel noise variance increases as the square of the FWHM, these authors determined that the optimal collimator resolution for estimating lesion *activity* corresponded to a FWHM ~0.4 times the disc diameter. This strict requirement on resolution results primarily from fitting for lesion *size*, as well as activity and background activity levels. (In fact, the resolution which optimized the precision of the estimates of lesion *size* in this 3-parameter problem was ~0.25 times the disc diameter!) Size estimation is an example of a higher-order task (Hanson 1983, 1984) which requires accurate information at higher image spatial frequencies. From this perspective, then, these optimal resolutions for the tasks studied seem not too surprising. These results were, essentially, independent of the proportionality constant relating count sensitivity to the square of the collimator resolution, as long as the ML parameter estimation procedure encountered no "convergence problems". In practice, this meant that the images had to contain a certain minimum number of counts, which depended on the lesion size (fewer total counts being adequate for convergence with larger lesions). Above this threshold number of counts for a given lesion size, however, the precision of parameter estimates simply scaled as the square root of the total image counts, and the optimal resolutions determined by the procedure were independent of count level.

Lastly, we mention another general aperture optimization method, which is based on maximizing the mutual information content of SPET images (Shao et al. 1989; Hero and Shao 1990). To our knowledge, this technique has not yet been applied to the design of a conventional gamma-camera collimator for optimal quantification.

Human observer performance in perceptual tasks

The simplest human observer perceptual task of possible relevance to nuclear medicine might be the detection of lesions of known size and shape in a noisy background of known amplitude. In such experiments, the observers typically have an unambiguous, low-noise "model" image available for direct comparison with all of the various noisy images which serve as the perceptual stimuli for the experiment. (Roughly half of the stimuli contain lesions). The observer simply scores the likelihood of a lesion of the same amplitude and size as that of the model image being present in each test image. A receiver-operator characteristic (ROC) curve of the observer's true-positive fraction vs. false-positive fraction for each criterion threshold may be fitted to obtain a perceptual signal-to-noise ratio for that observer's performance viewing the given set of images.

Wagner and Brown (1985) reviewed the performance of ideal observer calculations, which attempt to use all of the available image information to calculate a "physical" signal-to-noise ratio (SNR) for any hypothesized lesion. An ideal observer calculation is not meant to serve as a model for human perception but only as a standard against which human performance may be compared. This comparison might be expected to be legitimate within a domain limited to perceptual tasks of relatively low complexity. Nevertheless, to date, ideal observer calculations have been quite successful in predicting human performance under a wide range of different physical and display conditions (Barlow 1978; Tsui 1978; Tsui et al. 1978; Burgess et al. 1981, 1982; Judy et al. 1981; Judy and Swensson 1985; and many others). The physical SNR is usually calculated by cross-correlating a set of images with the expected lesion shape. The result of this calculation, a single scalar number from each image (the decision variable), has one distribution when the lesion is actually present and another, shifted

distribution when the lesion is absent. The difference in means of the two distributions compared with their widths may be used to define the physical SNR.

It might seem reasonable, therefore, to optimize collimation (or any other system component, for that matter) on the basis of simply maximizing the ideal observer SNR. However, Tsui et al. (1978) and Tsui (1978) discussed the absurd conclusion with this approach that the optimal collimator is, in fact, *no* collimator! In other words, if the signal to be detected and the background are known exactly by the observer in advance, then a simple measurement of total counts – even uncollimated counts – would suffice to indicate the presence or absence of a lesion. This seeming paradox was understood by modifying the model to include the observer's need to estimate the background level in order to "test" if the hypothesized lesion signal appears significantly different from it (Tsui et al. 1978). The modified model tracked the human observer performance well and indicated an optimal collimator resolution FWHM comparable with the lesion diameter.

Another metric that has been shown to correlate well with results of several observer performance studies is the so-called Hotelling trace (Hotelling 1931), which has been reintroduced and examined by Barrett and coworkers in recent years (1985, 1986). The Hotelling trace is an ideal linear discriminant calculation which is quite general in nature, making no assumptions concerning the method of "processing" of visual information performed by the observer. It has been applied to several complex perceptual tasks, including detection in the presence of variable background and signal (Fiete et al. 1987), collimator optimization for a 3-D liver SPET model (White et al. 1989) and detection in correlated, "lumpy" noise backgrounds (Myers et al. 1989). In these studies, the Hotelling trace correlated well in all cases, except for low noise and low contrast images, for which it has been argued that the human's "internal noise" becomes a more dominant source of uncertainty. For the lumpy background experiments, it was observed that the spatial resolution required for the best lesion detection performance improved with the degree of complexity of the noisy background.

Another higher-order perceptual task was described by Tsui et al. (1983). These authors demonstrated that the task of discriminating the size of two different lesions (i.e. determining which lesion is larger) also requires considerably better spatial resolution than does the simple detection task, as discussed above.

We have not yet explicitly considered another relevant complex perceptual task: the detection of lesions in *unknown locations*. This task requires the observer to search for the lesion(s). A successful ideal observer model for this task has only been derived for discrete, nonoverlapping locations (Swensson and Judy 1981). Models which have been proposed for the more general case (e.g. Wagner and Barrett 1987) have not been supported by data (Judy and Swensson 1988).

Special considerations for SPET

In planar projection images, the image noise is spatially uncorrelated from pixel to pixel. This means that the statistical noise of each pixel is entirely independent of the noise of all other pixels in the image. In frequency space, this kind of noise is said to be "white", because the noise power is "flat", i.e. distributed uniformly across all spatial frequencies in the images. By contrast, the statistical noise in tomographically reconstructed images is spatially *correlated* by the ramp filter used for reconstruction (Riederer et al. 1978; Kijewski and Judy 1987). For such correlated noise, the noise power spectrum (NPS) is not constant, or white, but rather is said to be "coloured" by the reconstruction process. In SPET, the non-stationary projection noise and attenuation compensation procedure also influence the shape of the NPS (Moore et al. 1988). The resulting spatial noise correlations lead to image noise "blotches" which can mimic real lesions. Thus, in many human perceptual studies with spatially correlated noise (e.g. Myers et al. 1985), it has been observed that the perceptual SNR is significantly less than one would expect based on an ideal observer SNR calculation. A simple "handicapping" of the model, i.e. removing the physical calculation's capacity to use knowledge of the noise correlations, restores its predictive value (Wagner and Brown 1985).

The apparent inability of the human to "see through" the noise correlations in tomographic images can be explained (Myers and Barrett 1987) in terms of spatial frequency "channels" known to exist in the human visual system. In optimizing the design of collimators for perceptual tasks on SPET (as opposed to planar) images, any task calculations should, therefore, be appropriately handicapped to account for the human observer's limitations in this regard.

Another important consideration for SPET collimator design is that the structures of interest in brain and heart slices are generally small, high-contrast features. Muehllehner (1985) demonstrated in a simulation study that the contrast of such a feature, or the signal to be detected, increases more rapidly with improving spatial resolution than the noise does, due to lower count sensitivity. Thus, for this case, there can be a net gain in SNR by using collimators of surprisingly good resolution.

This observation was confirmed in a study of two collimators for ^{123}I brain imaging (Mueller et al. 1986). These authors compared SPET images obtained with a high-resolution, long-bore (LB) collimator to those obtained with a LEGP collimator. Although the LB count sensitivity was much less than that of the LEGP, when the LB images were smoothed to have the same spatial resolution as the LEGP images, their percentage root mean square (rms) image noise was only about 0.6 times that of the latter. Superior clinical images were also achieved with the LB. The conclusions of this work

were similar to the results of an earlier study by Phelps et al. (1982) who showed that for two positron emission tomography (PET) systems providing equal count sensitivity and reconstructed spatial resolution, the system with many small detectors and a smooth reconstruction algorithm would significantly outperform the system with fewer, larger detectors and a sharper reconstruction filter. This concept was termed "signal amplification" by these authors.

It is clear that for a given collimator-detector combination, the best spatial resolution will be obtained when the collimator is as close to the patient as possible, so that b in Eqn. (1) is minimized. This motivated the development of special "cut-off" gamma-camera heads to clear the patient's shoulders for brain SPET (Larsson et al. 1984), as well as parallel slant-hole collimators (Polak et al. 1984) which permit angling the camera with the same consequences. The advent of SPET systems with multiple heads and fan-beam collimators has limited the application of these types of camera/collimator modifications primarily to single-headed systems.

Because the spatial resolution of a collimator worsens linearly with distance from the collimator, reconstructed SPET images usually demonstrate a non-uniform reconstructed spatial resolution, e.g. the resolutions in the circumferential and radial directions are significantly different. The non-stationarity of the 3-D PSF may be improved somewhat by taking the conjugate mean of opposing projections before reconstruction (Glick et al. 1989), which is often done as an integral part of various attenuation compensation procedures. In addition, many reconstruction algorithms to correct for this geometric non-stationarity have recently been described. The degree of non-stationarity over the tomographic FOV can also be minimized somewhat by increasing the bore length (thickness) of the collimator [a in Eqn. (1)]. To our knowledge, the optimal trade-off between collimator thickness and non-stationarity correction algorithms is still an open and interesting question for several quantitative and perceptual tasks of interest.

Practical considerations in collimator selection

Image quality is governed by how well the single photon imaging system physically achieves the principle of correspondence between the direction of gamma-ray emission and the point of detection. This is dependent on the design of the collimator(s), which in turn defines the 'lines', and on the precision with which the detector locates the 'point' of detection. Both sensitivity and resolution are affected by the practical implementation of this principle. For a modern gamma-camera and an acceptable sensitivity, the definition of the 'lines' is the more important factor; the designer's choice of collimator parameters and the user's decision as to which collimator to use are dependent on what is the most acceptable compromise for a given imaging task.

In accordance with the radiation protection principle of ALARA (as low as reasonably achievable), the dose received by the patient should be the lowest required to provide an adequate quality study (ICRP 1988). As discussed above, the total number of gamma-rays detected is also crucial for image quality due to the randomness inherent in radioactive decay and counting: the greater the number of gamma rays used, the better, because statistical fluctuations will be reduced. However, patient comfort and movement also impose practical restrictions and hence the importance of sensitivity.

Spatial resolution together with contrast and statistical noise govern lesion detectability. If the FWHM resolution is not small enough relative to the volume of a lesion or other structure of interest, the reconstructed anatomical representation will not correspond to the true physical extent and the reconstructed activity concentration will be underestimated; this is referred to as the partial volume effect. The extent of the partial volume problem is reduced as resolution improves, with a concomitant increase in lesion contrast.

Thus, in practice, the information content in the image(s) is dictated by the amount of administered radiopharmaceutical, collimator choice and total data acquisition time. Regulatory authorities set the maximum allowable amount of radiopharmaceuticals, although these levels vary in different countries. The total data acquisition time can be varied by the operator depending on the patient's physical condition and ability to cooperate and on patient load. Collimator choice is dependent on the allocated data acquisition time and on the clinical question to be answered, for example, whether the diagnostic task is resolution or count limited.

For a given imaging task, experience usually establishes a minimum number of total counts necessary for an acceptable quality. For a given total time, high-sensitivity collimators result in more counts by allowing a wider range of photon paths through their collimator holes. However, it is increasingly realised that it is the quality of the counts that is important, and therefore the recommendation is generally against the use of high-sensitivity collimators. Thus, the real practical choice is between general purpose (GP) and high-resolution (HR) collimators. Even here, the recommendation is to use HR collimators for SPET (Keyes et al. 1990), unless conditions suggest that unacceptably low count levels would ensue (e.g. from a single-headed system imaging a low-dose study for a limited time). Whilst it is generally true that a compromise between resolution and sensitivity is necessary, we also suggest that in reaching such a compromise, the resolution improvement be given a greater weight than the accompanying loss in sensitivity.

Whether with GP or HR collimators, the gamma-camera must be as close as possible to the patient during its orbit because, as stated earlier, the system planar resolution deteriorates with distance from the collimator. The quality of the counts can be further improved by using an asymmetric energy window for better scatter

rejection and therefore better contrast. Finally, as shown above for imaging activity distributions of limited spatial extent, the use of fan-beam collimators can improve both resolution and sensitivity.

Collimator choice in the context of multi-headed SPET

The realisation that any improvements in resolution necessitate a loss in sensitivity has led to the development of SPET systems with more than one gamma-camera (commonly three) surrounding the patient's head or body (Lim et al. 1980). The design goal of these three-headed systems is to acquire volumetric data with isotropic sampling and high sensitivity. Some of the increased sensitivity can be sacrificed in pursuing better resolution and hence reduced partial volume effects, better contrast and better quantitative accuracy.

The triangular arrangement also offers the advantage that the cameras can be positioned relatively close to the patient's head or body. The GE/CGR Neurocam, being a brain-dedicated instrument, has its three cameras forming a fixed triangular aperture on a rotating gantry. In order to accommodate the body, three-headed systems such as the Trionix Triad, Picker Prism and Toshiba GCA-9300A utilise bigger cameras and have an adjustable triangular aperture size. Hence, the smallest triangle that can be achieved for imaging the brain is greater than that of the Neurocam. Although with parallel-hole collimators, this leads to a degradation of spatial resolution, the use of fan-beam collimators can offset the loss (Tsui et al. 1986).

The gain in sensitivity achieved by using more than one camera simultaneously has given additional flexibility to collimator designers in reaching a compromise between sensitivity and resolution. Table 1 compares the manufacturer's construction specifications of collimators for the GE 400XCT single rotating camera and for the three-headed GE/CGR Neurocam. It should be noted that the septal thickness for all these collimators seems to be determined by manufacturing limitations rather than penetration effects.

Tables 2 and 3 provide comparisons for the corresponding sensitivity and resolution of these systems as measured at the Institute of Nuclear Medicine, University College and Middlesex School of Medicine (UCMSM), London. Planar sensitivity was measured using a ^{99m}Tc-point source in air at 10 cm from the face of the collimator and tomographic sensitivity, using a 20 cm diameter cylinder uniformly filled with ^{99m}Tc. A symmetric 20% energy window was used. The system planar resolution was measured using a ^{99m}Tc-point source in air at 10 cm from the face of the collimator and the tomographic resolution, using a ^{99m}Tc-point source in air at the centre of the FOV (NEMA 1986). The SPET data acquisition parameters were:
For the GE 400XCT: 13 cm radius of rotation, 64 projections, 128 × 128 matrix, zoom 2, corresponding to a pixel size of 1.6 mm. This rotation radius corresponds to the smallest value routinely achievable in brain scanning. The average radius for 39 patients as reported by Larsson et al. (1984) was 12.7 cm.
For the Neurocam: 12.25 cm radius of rotation, 128 projections, 128 × 128 matrix, corresponding to a pixel size of 2.0 mm.

Reconstructions were performed using the ramp filter. The Neurocam resolution is better than that of the GE 400XCT camera and will improve further (by

Table 1. Comparison of collimator design parameters for a single rotating gamma-camera (GE 400XCT) and a brain-dedicated, three-headed system (GE/CGR Neurocam)

		Hole diameter (mm)	Septal thickness (mm)	Hole length (mm)
GE 400XCT	GP	2.5	0.3	41
	HR	1.8	0.3	40
Neurocam	GP	1.8	0.2	31.5
	HR	1.4	0.2	31.5
	UHR	1.4	0.2	38.5

All collimators are low-energy, parallel-hole, hexagonal hole shape

Table 2. Comparison of planar and tomographic sensitivity for a single rotating gamma-camera (GE 400XCT) and a brain-dedicated, three-headed system (GE/CGR Neurocam)

Collimator	Planar sensitivity (cps/MBq)		Tomographic sensitivity (kcps/MBq·ml·cm)	
	GE 400XCT	Neurocam	GE 400XCT	Neurocam
General purpose (GP)	142	130 × 3	12.8	50.7
High resolution (HR)	82	75 × 3	7.6	30.0

Table 3. Comparison of system planar and reconstructed resolution in air at the centre of the field of view (FOV) of a single rotating gamma-camera (GE 400XCT) and a brain-dedicated, three-headed system (GE/CGR Neurocam)

Collimator	Planar resolution (FWHM mm)		Reconstructed resolution (FWHM mm)	
	GE 400XCT	Neurocam	GE 400XCT	Neurocam
GP	10.4	9.6	11.7	10.7
HR	8.3	7.9	9.8	9.0

FWHM, full width at half-maximum

about 1–2 mm) with the forthcoming ultra-high-resolution (UHR) collimators.

The increase in sensitivity offered by the multi-headed systems gives the user additional flexibility in choosing the data acquisition parameters. At the Institute of Nuclear Medicine, UCMSM, the HR Neurocam collimators are used for all technetium-99m hexamethylpropylene amine oxime (^{99m}Tc-HMPAO) studies unless the patient is restless, in which case the data acquisition time must be minimised. With such patients, a SPET study is often not possible using a single rotating camera. Table 4 provides a comparison of typical imaging protocols for ^{99m}Tc-HMPAO brain perfusion SPET used at the Institute of Nuclear Medicine, UCMSM, with a single rotating camera (GE 400 XCT) and the Neurocam. The average amount of injected activity for an adult is 740 MBq. With HR collimators, the data acquisition time is 35–45 min on the single camera and only 15 min on the Neurocam, and yet the total number of counts on the Neurocam is about 1.4× greater, thereby assuring greater statistical reliability and better image quality. If the same total counts were to be acquired, either the Neurocam acquisition time could be reduced to about 11 min or the administered activity could be reduced by 30%. If the patient can remain still for about 20 min (which is only about half the time required by a single camera) then the administered activity can be reduced even further. In restless patients where the acquisition time must be short, use of the Neurocam with GP collimators for 11 min yields 1.4× the total number of counts acquired with HR collimators in 15 min. Thus, for the same total counts, the Neurocam acquisition time could be reduced to about 8 min. In general, given a patient with a provisional diagnosis, and after assessment of his/her capability to cooperate during data acquisition, optimisation of the imaging protocol is possible. The ease of collimator change on the Neurocam is a practical advantage in this respect.

The following comparison between two brain-dedicated, multi-headed systems in terms of planar sensitivity per camera and planar resolution demonstrates how collimator design is essentially dependent on a compromise between these two parameters. Different manufacturers often choose a different compromise, and it is therefore important to identify the repercussions on imaging performance. The two systems are the Neurocam and the Osaka/Hitachi SPET 2000 which comprises four gamma-cameras in a square arrangement rigidly fixed in a rotating gantry (Kimura et al. 1990). The distance between the collimator surfaces of opposed cameras is 26 cm so that the radius of rotation is 13 cm compared with 12.25 cm for the Neurocam. The interdependence between sensitivity and resolution is exemplified in the case of the Osaka HR and GP collimators: the sensitivity of the GP collimator is 4.8× that of the HR, and hence its planar resolution in air at 10 cm (13.7 mm FWHM) is significantly worse than that of the HR (6.9 mm). The sensitivity of the Neurocam HR collimator is only 1.7× that of the Osaka HR, and its planar resolution is somewhat inferior (8.1 mm compared with 6.9 mm). On the other hand, although the sensitivity of the Osaka GP collimator is only 1.7× that of the GP Neurocam, its planar resolution is significantly worse (13.7 mm compared with 9.7 mm). In this case, for a sensitivity gain of 1.7×, the degradation of planar resolution appears unacceptable. Unfortunately, the reconstructed resolution cannot be directly compared because the Osaka values were obtained using a Wiener pre-filter and Ramachadran filter (Kimura et al. 1990) rather than a ramp filter only. Under these conditions, the FWHM in air at the centre of the FOV (i.e. 13 cm from the collimators) is quoted as 7.0 mm for HR and 13.0 mm for GP collimators. These values must result primarily from the effects of the resolution recovery (Wiener) filter, since the planar resolution at 10 cm is 6.9 mm and 13.7 mm, respectively.

Table 4. Comparison of imaging protocols for technetium-99m hexamethylpropylene amine oxime (^{99m}Tc-HMPAO) (740 MBq) brain perfusion SPET using a single rotating gamma-camera (GE 400XCT) and a brain-dedicated, three-headed system (GE/CGR Neurocam)

Parameter	GE 400XCT	GE/CGR Neurocam	
Collimators	HR	HR	GP
No. of views	64	128	128
Matrix size	128	64	64
Pixel size (mm)	3.2	4.0	4.0
Time per view (s)	30–40	20	15
Total time (min)	35–45	15	11
Counts per view (kcnts)	50	35	50
Total counts (kcnts)	3200	4480	6400

A further comparison between the Neurocam and another brain-dedicated device, the annular single-crystal camera, ASPECT (Genna and Smith 1988; Holman et al. 1990), demonstrates the effects of collimator design on tomographic sensitivity and reconstructed resolution. Unlike the Neurocam and the Osaka/Hitachi systems, ASPECT consists of a stationary annular NaI(Tl) crystal and a concentric, rotating collimator system which comprises three parallel-hole collimators viewing the head from three angles simultaneously. The collimator hole size is 1 mm, septal thickness 0.18 mm and length 24 mm compared with 1.4 mm, 0.2 mm and 31.5 mm, respectively, for the Neurocam HR collimators. For ^{99m}Tc, the tomographic volume sensitivity is 27.0 kcps/MBq·ml·cm, and the reconstructed spatial resolution in air is 8.2 mm at the centre of the FOV compared with 30.0 kcps/MBq·ml·cm and 9.0 mm, respectively, for the Neurocam.

The Toshiba GCA-9300A, one of the commercially available head and body systems, comprises three rectangular cameras with a 41×21 cm FOV and offers both parallel-hole and fan-beam collimators (Ichihara 1990;

Table 5. Tomographic sensitivity and reconstructed spatial resolution for the Toshiba GCA-9300A three-headed system (Ichihara et al. 1991)

Collimator	Reconstructed resolution in air at centre of FOV (FWHM mm)		Tomographic sensitivity (kcps/MBq ·ml·cm)
	Radius =132 mm for brain SPET	Radius =200 mm for body SPET	
Parallel GP	13.8	17.0	56.7
Parallel HR	10.0	13.2	32.4
Parallel SHR	8.6	11.0	19.7
Fan-beam HR	9.6	–	51.3
Fan-beam SHR	7.5	–	35.1
Fan-beam UHR	5.9	–	17.0

SPET, single photom emission tomography; SHR, super high resolution; UHR, ultra high resolution

Ichihara et al. 1991). The smallest radius of rotation (corresponding to the cameras being closest to each other, forming an equilateral triangle) is 13.2 cm; the largest radius of rotation is 30.7 cm. Of particular interest are the low-energy fan-beam collimators which are used for the head (FOV is 22 cm diameter ×21 cm): super-high-resolution (SHR) one made of lead and an ultra-high-resolution (UHR) one made of tungsten. The tomographic volume sensitivities for different collimators measured using a 20 cm diameter, uniformly filled cylinder are listed in Table 5 together with the reconstructed spatial resolution in air at the centre of the FOV (Ichihara et al. 1991).

Discussion and conclusions

A HR parallel-hole collimator yields better quality images than a more sensitive parallel-hole collimator. With the advent of multi-headed cameras and the consequential gain in sensitivity, the loss of sensitivity accompanying the use of HR and even UHR collimators should become more easily acceptable. In neuroactivation and neuroimaging studies with the GE/CGR Neurocam, the HR parallel-hole collimators were routinely employed (George et al. 1991). In the heart, use of the SHR parallel-hole collimators with the three-headed Toshiba GCA-9300A system gave superior image quality and still led to a gain in sensitivity of 1.8 × compared with a single camera fitted with a HR collimator (Nakajima et al. 1990).

New collimator designs introduced to improve SPET resolution include cast collimators which can be made with more uniform hole construction than the lead-foil type, while new designs for brain imaging include converging fan-beam collimators as well as cone-beam and astigmatic collimators with convergence in both dimensions. These improve both sensitivity and resolution compared with parallel-hole collimators.

With the increased sensitivity of the multi-headed imaging systems, issues of patient throughput, reduced radiation exposure and/or improved accuracy can be addressed separately. Reduction of the total administered activity will be of benefit to the patients, staff and public. Reduction in the data acquisition time will result in greater patient throughput. However, it is now possible to reach a compromise between the two which, in addition, will yield better image quality than currently achievable with a single rotating gamma-camera. Hence, with such high-sensitivity systems and with HR collimators, better quality SPET images can be obtained at a reduced total administered activity. It is anticipated that the role of SPET in routine and research studies will be enhanced.

References

Anger HO (1964) Scintillation camera with multichannel collimators. J Nucl Med 5:515–531

Barlow HB (1978) The efficiency of detecting changes of density in random dot patterns. Vision Res 18:637–650

Barrett HH, Smith WE, Myers KJ, Milster TD, Fiete RD (1985) Quantifying the performance of imaging systems. In: Schneider RH, Dwyer SJ (eds) Application of Optical Instrumentation in Medicine XIII. Proc Soc Photo-opt Instrumen Eng 535:65–69

Barrett HH, Myers KJ, Wagner RF (1986) Beyond signal-detection theory. In: Schneider RH, Dwyer SJ (eds) Application of Optical Instrumentation in Medicine XIV. Proc Soc Photo-opt Instrumen Eng 626:231–239

Beck RN, Redtung LD (1985) Collimator design using ray-tracing techniques. IEEE Trans Nucl Sci NS 32:865–869

Budinger TF (1990) Advances in emission tomography: quo vadis? J Nucl Med 31:628–631

Burgess AE, Wagner RF, Jennings RJ, Barlow HB (1981) Efficiency of human visual signal discrimination. Science 214:93–94

Burgess AE, Jennings RJ, Wagner RF (1982) Statistical efficiency: a measure of human visual signal-detection performance. J Appl Photogr Eng 8:76–78

Chang W, Li SQ, Williams JJ, Bruch PM, Wesolowski CA, Ehrhardt JC, Kirchner PT (1988) New methods of examining gamma camera collimators. J Nucl Med 29:676–683

Cullum ID, Brown NJG, Christmas P, Jarritt PH, Sefton JP, Short MD, Woods MJ (1991) A proposal regarding the management of SPECT uniformity correction. Nucl Med Commun 12:299–300 (abstract)

deVries DJ, Moore SC, Zimmerman RE, Mueller SP, Friedland B, Lanza RC (1990) Development and validation of a Monte Carlo simulation of photon transport in an Anger camera. IEEE Trans Med Imag 9:430–438

Fiete RD, Barrett HH, Smith WE, Myers KJ (1987) The Hotelling trace criterion and its correlation with human observer performance. J Opt Soc Am A 4:945–953

Genna S, Smith AP (1988) The development of ASPECT, an annular single crystal brain camera for high efficiency SPECT. IEEE Trans Nucl Sci NS 35:654–658

George M, Ring H, Costa DC, Kouris K, Jarritt PH, Ell PJ (1991) Neuroactivation and neuroimaging with SPET. Springer, Berlin Heidelberg New York

Gerber MS, Miller DW (1974) Parallel-hole collimator design. J Nucl Med 15:724–725

Gillen GJ, Hilditch TE, Elliott AT (1988) Nonisotropic point spread function as a result of collimator design and manufacturing defects. J Nucl Med 29:1096–1100

Glick SJ, King MA, Knesaurek K, Burbank K (1989) An investigation of the stationarity of the 3D modulation transfer function of SPECT. IEEE Trans Nucl Sci 36:973–977

Gullberg GT, Zeng ZL, Christian PE, Datz FL, Morgan HT (1991) Cone beam tomography of the heart using SPECT. Invest Radiol 26:681–688

Hanson KM (1983) Variations in task and the ideal observer. Proc Soc Photo-opt Instrumen Eng (Application of optical instrumentation in medicine XI), SPIE Proc 419:60–67

Hanson KM (1984) Optimal object and edge localization in the presence of correlated noise. Proc Soc Photo-opt Instrumen Eng, SPIE Proc 454:9–17

Heller SL, Goodwin PN (1987) SPECT instrumentation: performance, lesion detection, and recent innovations. Semin Nucl Med 17:184–199

Hero AO, Shao L (1990) Information analysis of single-photon emission computed tomography with count losses. IEEE Trans Med Imag 9:117–127

Holman BL, Carvalho PA, Zimmerman RE, Johnson KA, Tumeh SS, Smith AW, Genna S (1990) Brain perfusion SPECT using an annular single crystal camera: initial clinical experience. J Nucl Med 31:1456–1561

Hor G (1988) Myocardial scintigraphy – 25 years after start. Eur J Nucl Med 13:619–636

Hotelling H (1931) The generalization of Student's ratio. Ann Math Stat 2:360

Ichihara T (1990) Development of a high resolution SPECT system. Toshiba Med Rev 33:29–35

Ichihara T, Matsudaira M, Yamada M (1991) Basic development of the Toshiba digital gammacamera, model GCA-9300A. In: Hisada K (ed) An atlas of second generation SPECT. Maruzen Planning Network, Japan, pp 13–19

ICRP (1988) Publication 53. Radiation dose to patients from radiopharmaceuticals. Annals of the ICRP. Pergamon, Oxford

Jarritt PH, Ell PJ (1984) Gamma camera emission tomography – quality control and clinical applications. Alden, Oxford

Jaszczak RJ, Chang LT, Murphy PH (1979) Single photon emission computed tomography using multi-slice fan beam collimators. IEEE Trans Nucl Sci 26:610–618

Jaszczak RJ, Floyd CE, Manglos SH, Greer KL, Coleman RE (1986) Cone-beam collimation for single-photon emission computed tomography: analysis simulation and image reconstruction using filtered backprojection. Med Phys 13:484–489

Judy PF, Swensson RG (1985) Detection of small focal lesions in CT images: effects of reconstruction filters and visual display windows. Br J Radiol 58:137–145

Judy PF, Swensson RG (1988) Detectability of equally visible disks at unknown locations. Radiology 169(P):239

Judy PF, Swensson RG, Szulc M (1981) Lesion detection and signal-to-noise ratio in CT images. Med Phys 8:13–23

Keller EL (1968) Optimum dimensions of parallel-hole, multi-aperture collimators for gamma-ray cameras. J Nucl Med 9:233–235

Keyes JW, Fahey FH, Harkness BA (1990) Tips for high quality SPECT. SNM Computer and Instrumentation Council Newsletter

Kibby PM (1969) The design of multichannel collimators for radioisotope cameras. Br J Radiol 42:91–101

Kijewski MF, Judy PF (1987) The noise power spectrum of CT images. Phys Med Biol 32:565–575

Kimura K, Hashikawa K, Etani H, et al. (1990) A new apparatus for brain imaging: a four-head rotating gamma camera single-photon emission computed tomograph. J Nucl Med 31:603–609

Larsson SA, Bergstrand G, Bergstedt H, Berg J, Flygare O, Schnell PO, Andersson N, Lagergren C (1984) A special cut-off gamma camera for high-resolution SPECT of the head. J Nucl Med 25:1023–1030

Lim CB, Chang LT, Jasczcak RJ (1980) Performance analysis of three camera configurations for single photon emission computed tomography. IEEE Trans Nucl Sci 27:559–568

Lim CB, Walker R, Pinkstaff C, et al. (1986) Triangular SPECT system for 3-D total organ volume imaging: performance results and dynamic imaging capability. IEEE Trans Nucl Sci 33:501–504

Mather RL (1957) Gamma-ray collimator penetration and scattering effects. J Appl Phys 28:1200–1207

Metz CE, Atkins FB, Beck RN (1980) The geometric transfer function component for scintillation camera collimators with straight parallel holes. Phys Med Biol 25:1059–1070

Moore SC, Kijewski MF, Mueller SP, Holman BL (1988) SPECT image noise power: effects of nonstationary projection noise and attenuation compensation. J Nucl Med 29:1704–1709

Moyer RA (1974) A low-energy multihole converging collimator compared with a pinhole collimator. J Nucl Med 15:59–64

Muehllehner G (1985) Effect of resolution improvement on required count density in ECT imaging: a computer simulation. Phys Med Biol 30:163–173

Muehllehner G, Luig H (1973) Septal penetration in scintillation camera collimators. Phys Med Biol 18:855–862

Muehllehner G, Dudek J, Moyer R (1976) Influence of hole shape on collimator performance. Phys Med Biol 21:242–250

Mueller SP, Pollak JF, Kijewski MF, Holman BL (1986) Collimator selection for SPECT brain imaging: the advantage of high resolution. J Nucl Med 27:1729–1738

Mueller SP, Kijewski MF, Moore SC, Holman BL (1990) Maximum-likelihood estimation – a mathematical model for quantitation in nuclear medicine. J Nucl Med 31:1693–1701

Myers KJ, Barrett HH (1987) Addition of a channel mechanism to the ideal-observer model. J Opt Soc Am A 4:2447–2457

Myers KJ, Barrett HH, Borgstrom MC, Patton DD, Seeley GW (1985) Effect of noise correlation on detectability of disk signals in medical imaging. J Opt Soc Am A 2:1752–1759

Myers KJ, Wagner RF, Brown DG, Barrett HH (1989) Efficient utilization of aperture and detector by optimal coding. In: Schneider RH, Dwyer SJ, Jost RG (eds) Medical Imaging III: image formation. Proc Soc Photo-Opt Instrumen Eng 1090:164–175

Nakajima K, Hisada K, Matsudaira M (1990) Applications of a three-detector SPECT system in heart disease. Toshiba Med Rev 33:43–50

NEMA (1986) NU 1. Performance measurements of scintillation cameras. National Electrical Manufacturers Association, Washington DC

Newiger H, Jordan K (1985) Optimization of collimators for imaging positron emitters by a gamma camera. Eur J Nucl Med 11:230–234

Phelps ME, Huang SC, Hoffman EJ, Plummer D, Carson R (1982) An analysis of signal amplification using small detectors in positron emission tomography. J Comput Assist Tomogr 6:551–556

Polak JF, Holman BL, Moretti JL, Eisner RL, Lister-James J, English RJ (1984) I-123 HIPDM brain imaging with a rotating gamma camera and slant-hole collimator. J Nucl Med 25:495–498

Raeside DE (1976) Monte Carlo principles and applications. Phys Med Biol 21:181–197

Riederer SJ, Pelc NJ, Chesler DA (1978) The noise power spectrum in computed X-ray tomography. Phys Med Biol 23:446–454

Shao L, Hero AO, Rogers WL, Clinthorne NH (1989) The mutual information criterion for SPECT aperture evaluation and design. IEEE Trans Med Imag 8:322–336

Swensson RG, Judy PF (1981) Detection of noisy visual targets: models for the effects of spatial uncertainty and signal-to-noise ratio. Perception Psychophysics 29:521–534

Tsui BMW (1978) Letter. Phys Med Biol 23:1203

Tsui BMW, Metz CE, Atkins FB, Starr SJ, Beck RN (1978) A comparison of optimum detector spatial resolution in nuclear imaging based on statistical theory and on observer performance. Phys Med Biol 23:654–676

Tsui BMW, Metz CE, Beck RN (1983) Optimum detector spatial resolution for discriminating between tumor uptake distributions in scintigraphy. Phys Med Biol 7:775–788

Tsui BMW, Gullberg GT, Edgerton ER, et al. (1986) Design and clinical utility of a fan beam collimator for SPECT imaging of the head. J Nucl Med 27:810–819

Wagner RF, Barrett HH (1987) Quadratic tasks and the ideal observer. Proc SPIE 767:306–308

Wagner RF, Brown DG (1985) Unified SNR analysis of medical imaging systems. Phys Med Biol 30:489–518

White TA, Barrett HH, Cargill EB, Fiete RD, Ker M (1989) The use of the Hotelling trace to optimize collimator performance (abstract). J Nucl Med 30:892